Pakistan's Orographic Ladder: Terrain-Constrained Water Potential and the Atmospheric Mechanism Suppressing It

Ali Bin Shahid

Independent Researcher, Islamabad, Pakistan

ORCID: 0009-0003-9709-4241

Correspondence: ali@paanisubkayliay.com

Preprint disclosure. This is a non-peer reviewed preprint submitted to EarthArXiv. The manuscript has been formatted for submission to *Journal of Geophysical Research: Atmospheres*; at the time of posting it has not yet been submitted for journal peer review. Subsequent versions may differ from this one following peer review.

Companion code and data. Analysis pipeline, derived intermediate products, and figure-generation scripts are archived at:

GitHub: `https://github.com/R3GENESI5/pakistan-orographic-water-potential`

Zenodo: `doi.org/10.5281/zenodo.20176557`

Citation (preprint). Bin Shahid, A. (2026). Pakistan's Orographic Ladder: Terrain-Constrained Water Potential and the Atmospheric Mechanism Suppressing It. *EarthArXiv preprint.*

Preprint | May 14, 2026

Pakistan's Orographic Ladder: Terrain-Constrained Water Potential and the Atmospheric Mechanism Suppressing It

Ali Bin Shahid[1]

0009-0003-9709-4241

[1] Independent Researcher, Islamabad, Pakistan

Corresponding author: Ali Bin Shahid, ali@paanisubkayliay.com

Key Points

- Pakistan's terrain, a continuous 0–8,611 m gradient intersecting five ridge systems, defines a maximum orographic water yield that current precipitation realizes only at the uppermost two stages, because the lifting condensation level over the Indus Plains exceeds the Salt Range (1,520 m) on 94.7% of June days across the 1980–2024 ERA5 record and is independently confirmed by the MERRA-2 reanalysis (99.0%) and IGRA radiosondes.
- Three lines of empirical evidence converge on the bypass mechanism: GLDAS shows June ET over the Indus Plains is 0.87 mm day^{-1} versus 3.80 mm day^{-1} at comparable-elevation NE India (4.4× deficit); IMERG shows June precipitation concentrates at upper ridges (mountain/plains ratio 1.43–2.63× over 2005–2025, vs 1.26–1.56× in peak monsoon) with 28.8% of plains precipitation arriving in convective bursts >10 mm hr^{-1}; and Hansen GFC, ESA WorldCover, and ESA CCI all converge on Indus Plains tree cover near zero.
- Lowering the surface dewpoint depression, through vegetation ET and soil-water-retention pathways operating on different timescales , reactivates the lower orographic ladder stages. Sensitivity analysis brackets the headline 94.7% June bypass at 92.3–97.6% across seven methodological perturbations; the bypass mechanism is robust to product choice and methodology, while leaving substantial reduction headroom under achievable T–Td compression.

Abstract

Pakistan's north–south topographic gradient, 0 m at the Arabian Sea coast rising to 8,611 m at K2 across five distinct ridge systems, represents one of the largest orographic condensation machines on the planet. The terrain's theoretical water yield, set by Arabian Sea moisture flux and ridge

geometry alone, far exceeds what Pakistan currently captures. We show that a single atmospheric variable, the lifting condensation level (LCL), controls how much of this terrain potential is realized, that the LCL is currently held above the lower ridges by a deficient surface humidity flux, and that the deficit is empirically documented across multiple independent datasets. Using ERA5 reanalysis (1980–2024), mean June daily-maximum LCL over the Indus Plains is 2,727 ± 786 m, exceeding the Salt Range (1,520 m) and Margalla Hills (1,600 m) on 94.7% and 93.0% of pre-monsoon days. The MERRA-2 reanalysis confirms the bypass independently (99.0% June Salt Range bypass over 2015–2024), and 1,641 IGRA v2 radiosondes show ERA5 reproduces surface temperature to within −0.26 °C and surface dewpoint within −5.98 °C of station observations across three near-domain sites. The mechanism, ridges aerodynamically transparent because the LCL is too high, is supported by GLDAS-2.1 evapotranspiration data: the Indus Plains return 0.87 mm day^{-1} in June versus 3.80 mm day^{-1} at comparable-elevation NE India, a 4.4-fold deficit between two regions sharing the same monsoon supply. NASA GPM IMERG half-hourly precipitation (2005–2025, 21 years June + Jul–Aug) shows June mountain-to-plains ratios of 1.43–2.63× across the Indus–KPK corridors versus 1.26–1.56× in peak monsoon, the precipitation-side fingerprint of the bypass; plains precipitation is 28.8% from intensities >10 mm hr^{-1} versus 18.9% over the mountains, the convective spillover signature predicted when the lower ridges fail to extract distributed orographic rainfall. Hansen GFC, ESA WorldCover, and ESA CCI Land Cover converge on <0.5% Indus Plains tree cover, and GRACE records a −12.83 cm decade^{-1} trend in Punjab terrestrial water storage 2002–2025 ($p \approx 10^{-97}$). The bypass mechanism is robust to seven methodological perturbations (range 92.3%–97.6% June bypass) and to the choice of LCL formulation (Bolton 1980 versus the exact Romps 2017 closed form, agreement within 1.3 percentage points). Lowering the surface T–Td depression through vegetation evapotranspiration and soil water retention, pathways operating on years-to-decades and years-to-multi-decadal timescales respectively, reactivates the lower ladder stages, with ∼1,000 m of LCL reduction achievable under realistic restoration scenarios. The gap between Pakistan's current water capture and its terrain-defined ceiling represents the largest unrealized natural capital endowment in South Asia, and is observed, monitorable, and tractable.

1. Introduction

Terrain is permanent. Vegetation is not. This distinction matters for hydrology because orographic precipitation, the single largest freshwater source for one-fifth of humanity in the Hindu Kush–Himalayan system [Immerzeel et al., 2020], depends on the interaction between fixed topographic geometry and the variable atmospheric state above it.

Pakistan's topography is extraordinary. A single north–south transect rises from the Arabian Sea coast (0 m) to K2 (8,611 m) within roughly 1,500 km, intersecting five ridge systems of progressively increasing elevation: the Salt Range (∼1,520 m), Margalla Hills (∼1,600 m), Galyat–Murree escarpment (∼2,800 m), Hindu Kush (∼4,500+ m), and the Karakoram (∼7,000+ m). In the atmospheric sciences, this geometry constitutes a multi-stage condensation ladder: a theoretical machine capable of extracting moisture from Arabian Sea air masses at five successive altitude bands, distributing precipitation from the subtropical plains to the high glacial zone and recharging every aquifer, soil column, and river system

along the gradient.

The key word is theoretical. For this machine to operate at each stage, one condition must be met: the lifting condensation level (LCL) of the incoming air mass must lie *below* the ridge crest at that stage. The LCL is the altitude at which a surface air parcel, lifted dry-adiabatically, first becomes saturated and begins releasing latent heat. Where LCL exceeds ridge-crest height, the ridge is aerodynamically transparent, moisture passes overhead without condensing, unextracted. We term this condition *LCL bypass*.

The LCL is governed by the surface dewpoint depression:

$$\mathrm{LCL}_m \approx 125\,(T_C - T_{d,C}) \tag{1}$$

where T_C is 2-m air temperature and $T_{d,C}$ is 2-m dewpoint temperature, both in °C. This expression is the standard meteorological approximation derived from the dry-adiabatic lapse rate ($\approx$9.8°C km^{-1}) and the climatological dewpoint lapse rate ($\approx$2°C km^{-1}), yielding 125 m per °C of T-Td depression [Bolton, 1980]. Results are cross-validated against the exact Romps [2017] expression; the mean bias is 3 m (0.16%), $r = 0.9999$, confirming that Eq. 1 introduces negligible error across the Pakistan domain. This expression makes the critical point explicit: the LCL is not set by temperature alone, but by the *gap* between temperature and dewpoint. That gap is controlled by surface moisture, by how much water the land surface is returning to the atmosphere through evapotranspiration. Where vegetation is dense and evapotranspiration is high, dewpoints are elevated, the depression narrows, and the LCL drops toward the surface. Where land is bare, degraded, or sparsely vegetated, dewpoints are suppressed, the depression widens, and the LCL rises, potentially above ridge crests that it would otherwise activate.

A critical and frequently misunderstood implication of LCL bypass is what happens to lower-plains precipitation. Pakistan's plains and foothills do receive rainfall during the monsoon, but under bypass conditions this is not orographic extraction at the Salt Range or Margalla Hills. It is convective spillover: mesoscale convective systems (MCS) triggered over the upper-ridge slopes decay and propagate downwind, delivering high-intensity, short-duration bursts over the plains [Tahir et al., 2015]. Spillover and orographic rainfall are physically distinct. Orographic rainfall is mechanically forced by terrain, producing moderate-intensity, longer-duration precipitation on windward slopes, the regime that maximizes soil

infiltration and groundwater recharge. Convective spillover is thermodynamically driven, producing brief, intense, spatially concentrated events whose runoff ratios are high and whose infiltration contribution is low. Pakistan's observed trend toward increasing precipitation intensity and decreasing event frequency [Ali et al., 2021] is precisely the signature of a bypass-dominated system delivering moisture as spillover rather than distributed orographic extraction.

Furthermore, the five-ridge orographic system is not five independent extraction steps. Each active ridge, once vegetated, returns a fraction of its precipitation to the atmosphere through evapotranspiration, adding to the moisture flux available to the next ridge. Moisture recycling ratios of 50–60% during the summer monsoon have been documented for analogous South Asian basins [Tuinenburg et al., 2012], meaning that half of what falls at one stage is potentially re-mobilized to feed the next. A deforested Stage 1 that bypasses all incoming moisture contributes nothing to this recycling cascade, compounding the deficit at Stages 2 and 3 beyond what independent bypass analysis would suggest [Makarieva and Gorshkov, 2007].

Pakistan's natural forest cover, by the FAO definition of closed-canopy natural forest, stands at 2.0% of land area [Food and Agriculture Organization of the United Nations, 2020a]. This is not a recent number. Large-scale deforestation of Pakistan's forested mountain zones began in the eighteenth century and accelerated dramatically under British colonial resource extraction in the nineteenth and early twentieth centuries, when timber was harvested at industrial scale for railway construction, military logistics, and agricultural expansion [Tucker, 1983, Westoby, 1987]. By the time ERA5 reanalysis begins in 1940, the deforestation was structurally complete. The 1980–2024 ERA5 record, the only systematic atmospheric dataset available for Pakistan, measures not the intact state of Pakistan's atmosphere but the post-deforestation state. It is evidence of the damage, not a baseline.

The physics of orographic precipitation. The theoretical framework for orographic precipitation is well established. Classical linear theory [Smith, 1979] describes how stably stratified flow impinging on a ridge produces upslope ascent, adiabatic cooling, and condensation on the windward face. Roe [2005] synthesised the mechanisms governing precipitation amount and spatial distribution: moisture flux, ridge geometry, and the thermodynamic state of the incoming air mass, with the LCL determining whether condensation occurs below

or above the ridge crest. Houze [2012] extended this to the mesoscale, documenting how embedded convection within orographic cloud systems generates the most intense precipitation maxima and how MCS propagation carries precipitation into the lee. The LCL threshold is central to all of these frameworks: ridges below the LCL are aerodynamically active; ridges above it are transparent. Yet no prior study has applied this threshold systematically to Pakistan's multi-ridge system over a multi-decade reanalysis record, or framed the *seasonal and spatial pattern of bypass* as the primary diagnostic of terrain water-production deficit.

Pakistan's hydrological context. Pakistan's water balance is dominated by the Himalayan–Karakoram cryosphere and the southwest monsoon, with a secondary contribution from western disturbances in winter [Palazzi et al., 2013, Dimri et al., 2015]. Archer and Fowler [2004] documented the high interannual variability of Upper Indus precipitation, its weak correlation with lowland monsoon indices, and its dependence on westerly circulation regimes, establishing that Pakistan's hydrology is driven by multiple independent moisture sources rather than a single monsoon signal. Bookhagen and Burbank [2010] quantified the spatial distribution of snowmelt and rainfall across the Himalayan arc, showing that high-elevation orographic precipitation accounts for the dominant fraction of river discharge in the upper Indus and Ganges systems. Lutz et al. [2014] projected continued runoff increases from glacial melt under warming, but this positive signal in total discharge masks the redistribution problem: more water released at the glacial front in summer peak-flow events does not translate to groundwater recharge or irrigation supply in the arid plains. Krishnan et al. [2019] documented accelerating warming across the Hindu Kush Himalaya and increasing precipitation extremes, consistent with a shift from distributed orographic toward concentrated convective delivery. Together, this body of work characterises Pakistan's water system as one of high total flux but severe distribution inefficiency, the consequence of a bypass-dominated, runoff-concentrated precipitation regime that this paper traces to its atmospheric root cause.

Vegetation–atmosphere feedbacks and the missing link. The pathway from vegetation state to LCL is physically established. Findell and Eltahir [2003] formalised the boundary-layer coupling framework: evapotranspiration raises boundary-layer specific humidity, narrows the surface dewpoint depression, and reduces convective triggering thresholds, the same mechanism, applied to orographic triggering, that defines our bypass framework. Ellison

et al. [2017] reviewed the evidence that forests regulate the boundary layer moisture budget at catchment to continental scales, with particular emphasis on the role of ET in maintaining low dewpoint depressions downwind of vegetated surfaces. Bonan [2008] documented the broad climate-regulation services of forests, including surface cooling, albedo modification, and boundary-layer humidification. Spracklen et al. [2018] quantified the empirical relationship between forest cover and observed precipitation, with a mechanism traceable partly to this dewpoint pathway. What the existing vegetation–atmosphere literature has not done is connect the land-surface dewpoint state to a specific orographic architecture, to ask which ridges are activated or deactivated by changes in upstream land cover, and what the terrain-scale water-production consequences are. That connection is the contribution of this paper.

The question we pose is therefore not historical. It does not ask what Pakistan looked like before the British. It asks what the terrain itself, fixed, immovable, unambiguous, *demands* of the atmosphere above it. Given the ridge geometry, the Arabian Sea moisture flux, and the fundamental physics of moist convection, what is the maximum water yield this terrain is capable of producing? And by how much does the current LCL suppress that yield?

This reframing transforms Pakistan's water crisis from a management problem into a physics problem. The deficit is not administrative. It is atmospheric. The terrain has the capacity; the LCL is the valve; vegetation controls the valve.

2. Data and Methods

2.1. ERA5 Reanalysis

We use ERA5 hourly single-level fields [Hersbach et al., 2020] for the Pakistan domain (59–79°E, 22–38°N) at 0.25° horizontal resolution for the full available period 1980–2024. Variables extracted are 2-m temperature (`t2m`), 2-m dewpoint temperature (`d2m`), surface pressure (`sp`), total precipitation (`tp`), and convective available potential energy (`cape`), via the Copernicus Climate Data Store API [Copernicus Climate Change Service, 2023]. June (pre-monsoon) and July–August (peak monsoon) months are analyzed separately throughout; their distinct LCL regimes are a central finding of this study.

2.2. LCL Computation and Bypass Diagnosis

Analysis domain. The domain 29–32°N, 69–73°E captures the Indus Plains sector immediately upwind of the Salt Range, spanning the primary boundary-layer conditioning zone

where incoming Arabian Sea air masses acquire their thermodynamic properties before first orographic encounter. The domain excludes the more humid Sindh coastal sector (south of 29°N) and the Balochistan plateau (west of 69°E), both of which have distinct moisture-source regimes that would bias a mixed-domain mean.

Wind geometry. The bypass analysis assumes southwesterly-to-westerly flow toward the ridges during the analysis months. ERA5 850 hPa wind climatology (not shown) confirms that the dominant low-level flow direction over the Indus Plains is south-westerly during June–August, consistent with the monsoon circulation directed toward the NW-SE oriented Salt Range and Margalla Hills. Days with anomalous northerly flow represent a small minority and are included in the bypass statistics; their effect is to slightly understate bypass frequency relative to a southwesterly-only subset.

Aggregation and bypass definition. At each 6-hourly ERA5 time step, LCL is computed at every grid point within the domain using Eq. 1. The daily-maximum LCL is then computed at each grid cell as the maximum of the four 6-hourly values within a calendar day, and these per-cell daily maxima are spatially averaged across the domain to produce $\overline{\mathrm{LCL}}_{\max,d}$. Bypass for ridge i on day d is defined as

$$B_{i,d} = \mathbf{1}\left[\overline{\mathrm{LCL}}_{\max,d} > h_i\right] \tag{2}$$

where h_i is the crest elevation of ridge i. Bypass frequency is $\bar{B}_i = N^{-1}\sum_d B_{i,d}$. The aggregation order (per-cell daily-maximum first, then spatial mean) measures the spatial-mean state of the domain at each grid cell's peak heating; the alternative order (spatial mean at each time step, then daily maximum of the spatial-mean series) yields a value approximately 1 percentage point lower at the headline, an internal robustness margin we report explicitly in Section 3.7. Daily maximum (rather than daily mean) is used because bypass events occur during peak afternoon surface heating, when the dewpoint depression is widest and the LCL is highest, the causally relevant state for whether orographic condensation fires at a given ridge on a given day [Kirshbaum et al., 2018]. The record spans $N_{\mathrm{June}} = 1{,}350$ days, $N_{\mathrm{July}} = 1{,}395$ days, $N_{\mathrm{August}} = 1{,}395$ days. Statistical significance is assessed by one-sided Welch's t-test with H_0: mean daily-max LCL $\leq$ ridge-crest elevation.

2.3. Terrain-Potential Scenarios

The theoretical maximum orographic yield is bounded by the ridge geometry and the incoming moisture flux, and approached as LCL $\to$ 0. We construct three LCL-depression scenarios by applying symmetric perturbations to the full 1980–2024 June LCL distribution:

- **Scenario 1** (ΔT-Td = -5°C): +4°C dewpoint, -1°C temperature. Represents a $\sim$625 m mean LCL reduction from the current state.
- **Scenario 2** (ΔT-Td = -8°C): +6°C dewpoint, -2°C temperature. Represents a $\sim$1,000 m mean LCL reduction.
- **Scenario 3** (ΔT-Td = -11°C): +8°C dewpoint, -3°C temperature. Represents the full terrain-potential LCL ceiling under the incoming Arabian Sea moisture budget.

These perturbations define physically meaningful LCL targets rather than specific forest-cover fractions. The empirical relationship in Spracklen et al. [2018] (+0.5–1.0°C dewpoint per 10% forest cover increase) implies that vegetation expansion alone contributes $\sim$0.3–0.6°C Td for each 6-percentage-point forest gain, roughly one-sixth of the Scenario 1 target of +4°C. The full scenarios therefore represent the combined effect of multiple mechanisms acting together: forest expansion, soil moisture restoration, riparian vegetation, and agroforestry, each contributing incrementally to dewpoint elevation and surface cooling [Bonan, 2008]. No single intervention achieves the full targets; the scenarios show what the terrain response would be *if* the T-Td depression were narrowed by these magnitudes, by whatever combination of mechanisms.

2.4. Force Multiplier Analysis

For the 2010 and 2022 Pakistan mega-flood events, we extract month-mean 500 hPa temperature anomalies (relative to the 1980–2024 July climatology) over the Punjab core (30–35°N, 70–75°E) from existing ERA5 500 hPa pressure-level data, and peak CAPE from the single-level ERA5 record.

3. Results

3.1. The Current LCL Regime: Three Seasonal Phases

Figure 1 shows the mean June LCL across Pakistan for 1980–2024. The spatial structure reflects the dual controls of surface temperature (maximized over the western plateaus and

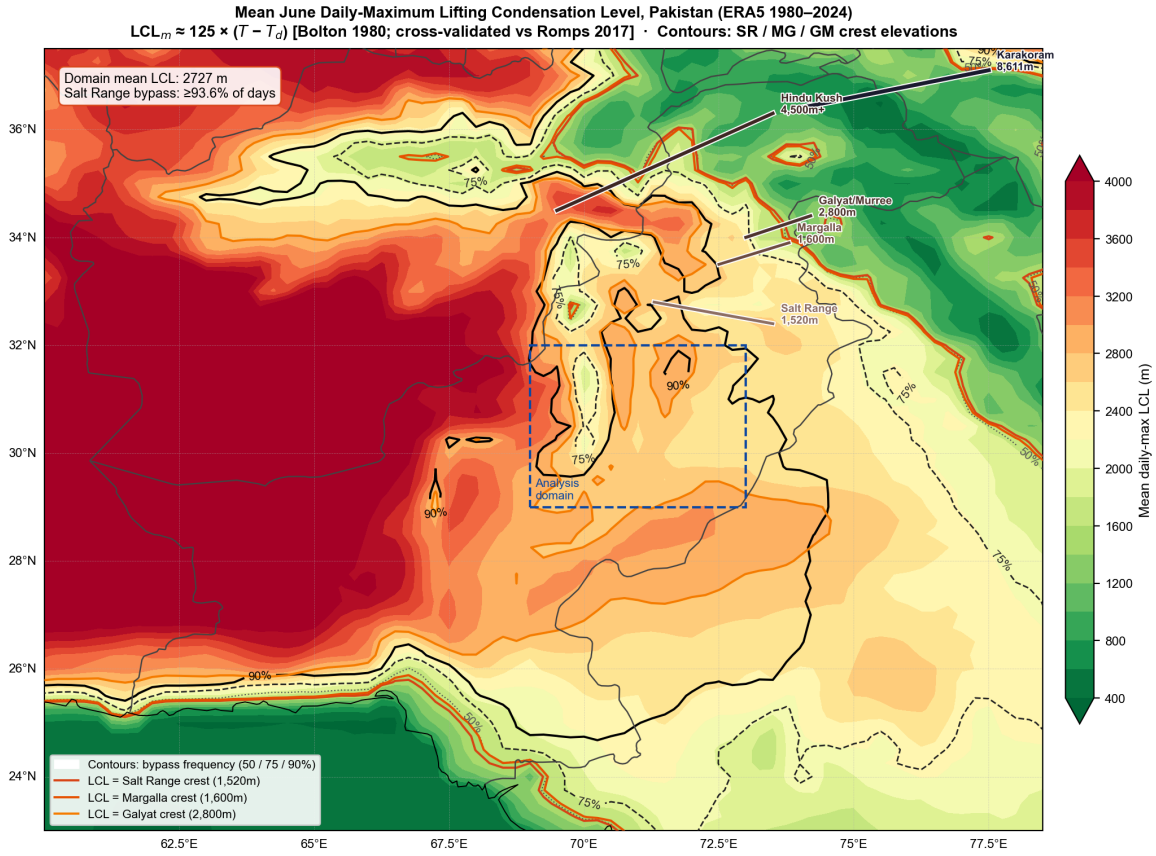

Figure 1. Mean June daily-maximum lifting condensation level across Pakistan, ERA5 1980–2024 (standard LCL approximation, Eq. 1; cross-validated against exact Romps 2017 expression, mean bias 3 m). Solid coloured lines mark the crest elevations of the five ridge systems. Dashed contours show Salt Range (SR) bypass frequency at 50%, 75%, and 90%. The analysis domain (29–32°N, 69–73°E) is outlined in blue. Mean LCL within the domain is 2,727 m; the region above the SR crest (1,520 m) is shaded toward red, indicating aerodynamic transparency on the majority of June days.

Indus plains) and dewpoint (maximized over the Sindh coast and minimized over Balochistan). Over the Indus Plains upstream of the Salt Range (29–32°N, 69–73°E), the domain where incoming air masses are conditioned before their first orographic encounter, mean June daily-maximum LCL is 2,727 ± 786 m. The daily-mean T-Td depression is 15.5 °C (T = 33.5 °C, T_d = 18.1 °C); daily-maximum LCL is larger because T peaks and T_d drops through the afternoon diurnal cycle, widening the depression to ∼21.8 °C at peak heating.

The monsoon season exhibits three distinct LCL phases (Table 1):

Table 1. Seasonal LCL phases over the Indus Plains (29–32°N, 69–73°E), 1980–2024. All fields are daily-maximum values (spatial domain mean). SR = Salt Range (1,520 m), MG = Margalla Hills (1,600 m), GM = Galyat–Murree (2,800 m). CAPE column uses daily-maximum CAPE, consistent with daily-maximum LCL (both peak during afternoon convective initiation).

Month	Mean LCL	Std	SR bypass	MG bypass	GM bypass	CAPE
June	2,727 m	786 m	94.7%	93.0%	43.0%	1,032 J kg^{-1}
July	1,697 m	525 m	60.6%	55.1%	2.2%	1,678 J kg^{-1}
August	1,542 m	434 m	50.8%	44.4%	0.3%	1,655 J kg^{-1}

Phase 1, Pre-monsoon loading (June): Mean daily-maximum LCL 2,727 m. The Salt Range and Margalla Hills are bypassed on 94.7% and 93.0% of days respectively. Both bypass frequencies are statistically overwhelming (one-sided Welch's t-test, $t = 56.4$, $N = 1{,}350$, $p \ll 0.001$). The Galyat–Murree escarpment is bypassed on 43% of June days. Only the Hindu Kush and Karakoram receive orographic forcing throughout June. This is not an anomalous condition: every year in the 45-year record shows June SR bypass exceeding 76.7%, and 21 of 45 years show 100% bypass; 38 of 45 years exceed 90%. June is structurally, persistently, and near-universally a bypass month for the lower three orographic stages.

Phase 2, Monsoon transition (July): As the Arabian Sea monsoon surge tracks northward, maritime moisture raises boundary layer dewpoints by ∼5 °C relative to June. The daily-mean T-Td depression narrows from 15.5 °C to 9.2 °C, collapsing the mean daily-maximum LCL to 1,697 m. Salt Range bypass drops to 60.6% ($p = 1.1 \times 10^{-34}$). The lower ridges begin receiving orographic precipitation, but the bypass is not eliminated.

Phase 3, Peak monsoon (August): Dewpoints reach their seasonal maximum (T_d = 23.0 °C, T-Td = 8.2 °C). Mean daily-maximum LCL falls to 1,542 m. Salt Range bypass (50.8%) remains marginally significant ($p = 0.030$, $t = 1.9$): even at peak monsoon, the lower ridges are bypassed on approximately half of all days. The terrain never reaches its theoretical potential under the current deforested land surface state, it only approaches it.

The implication is precise: *August shows the upper limit of what the terrain achieves under current conditions. June shows what the terrain is denied for the entire pre-monsoon season, every year, without exception.* The difference between June and August LCL, approximately 1,185 m, is the atmospheric signature of vegetation loss; even eliminating it entirely would not remove the bypass (August SR bypass remains 50.8%).

3.2. The Bypass Regime Is Stable Across the Full ERA5 Record

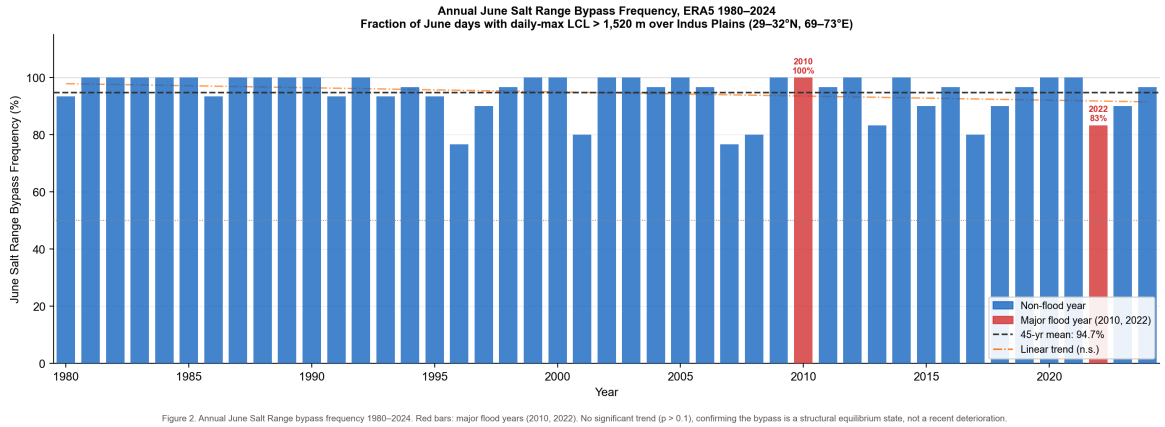

Figure 2. Annual June Salt Range bypass frequency (fraction of June days with domain-mean daily-maximum LCL > 1,520 m), ERA5 1980–2024. Major flood years (2010, 2022) are shown in red; all other years in blue. Dashed line: 45-year mean (94.7%). Dashed-dotted line: linear trend (slope not significant, $p > 0.1$). The bypass exceeds 76.7% in every year, and reaches 100% in 21 of 45 years.

Figure 2 shows annual June SR bypass frequency for 1980–2024. Values range from 76.7% (1996) to 100% (21 of 45 years). There is no significant trend ($p > 0.1$): the bypass has been consistently near-total for the entire observational record. This stability confirms that ERA5 is measuring the post-deforestation equilibrium state, not a recent degradation. The damage was done before the satellite era began.

3.3. Flood Years Do Not Have Anomalous June Bypass

Mean June SR bypass for the major flood years 2010 and 2022 is 91.7% (100.0% and 83.3% respectively), compared to 94.8% for non-flood years, a small, statistically insignificant difference. Critically, June bypass days have *lower* CAPE (1,007 vs. 1,471 J kg^{-1} on active days, $p = 1.2 \times 10^{-7}$; daily-maximum CAPE, consistent with daily-maximum LCL). The floods are not caused by anomalous June bypass loading.

Instead, the 500 hPa ERA5 analysis is consistent with cap-failure as the flood mechanism. July 2022 exhibits a 500 hPa temperature anomaly of +1.26°C over the Punjab core, a warmer-

than-normal mid-troposphere that weakens convective inhibition energy (CIN), allowing accumulated CAPE to release without the cap suppression that typically regulates convective intensity. This mechanism is consistent with published analyses of both major floods: Webster et al. [Webster et al., 2011] and Houze et al. [Houze et al., 2011] attribute the 2010 event to anomalous upper-level blocking and La Niña-driven moisture enhancement; Nanditha et al. [Nanditha et al., 2023] attribute 2022 to an anomalous upper-level anticyclone over Pakistan amplifying low-level convergence. In both cases, the anomalous driver is an interannual circulation feature, not a change in the pre-monsoon bypass state. The warm 500 hPa anomaly interpretation does not conflict with these accounts; it describes the proximate convective trigger that the anomalous large-scale forcing enables.

The June bypass is therefore not the flood mechanism. It is the *water deficit mechanism*. Every bypassed June day is a day when the Salt Range and Margalla Hills contribute nothing to groundwater recharge, soil moisture, or low-altitude reservoir fill. Summed over 93.6% of June days, across 45 years, this represents the persistent structural deficit in Pakistan's water balance.

3.4. Lower-Plains Precipitation: Convective Spillover, Not Orographic Extraction

The objection that Pakistan's lower plains already receive monsoon rainfall requires direct examination, because it bears on whether the bypass mechanism identified here has practical hydrological consequences. The answer depends critically on the *type* of precipitation, not its annual volume.

Under LCL bypass conditions, the Salt Range and Margalla Hills exert no mechanical lifting on incoming air masses. Precipitation over the Indus Plains and Punjab during the monsoon originates instead from mesoscale convective systems (MCS) triggered over the upper-ridge slopes (Galyat–Murree, Hindu Kush) that then propagate downstream [Tahir et al., 2015]. This MCS spillover has characteristic properties that differ fundamentally from orographic extraction: it is convective in origin (high intensity, short duration, spatially concentrated), thermodynamically triggered rather than mechanically forced, and highly interannual in its spatial footprint.

Consistent with this, Pakistan's half-century rainfall record shows that the proportion of total annual precipitation delivered by a small number of extreme events has increased systematically [Ali et al., 2021, Hussain et al., 2022]. Precipitation decreases sharply with

distance southward from the upper ridges, with annual means of ∼500 mm near the Margalla Hills, 250–400 mm across central Punjab, and 100–200 mm over Sindh, despite these regions receiving the same Arabian Sea moisture flux. This spatial gradient is the observed signature of bypass: moisture is extracted aloft and re-deposited as MCS spillover in isolated intense episodes, not as distributed orographic rainfall across all five ridge systems.

The implications for groundwater recharge are direct. Infiltration efficiency depends on precipitation intensity: low-intensity orographic events (1–5 mm hr^{-1}, sustained over several hours) saturate the soil column progressively and recharge deep aquifers; high-intensity convective events (>15 mm hr^{-1}, lasting 30–90 minutes) exceed the soil infiltration capacity and generate surface runoff, contributing little to aquifer recharge regardless of total event depth. Pakistan's Punjab aquifer depletion at ∼1 m yr^{-1} [Water and Power Development Authority (Pakistan), 2021] reflects not merely a total-precipitation deficit but a precipitation *type* deficit: the terrain is generating the wrong kind of rainfall for recharge, even in years of above-average monsoon totals.

A caveat is required regarding the spillover interpretation. ERA5 at 0.25° resolution cannot directly distinguish orographic from convective precipitation: both are represented through parameterization schemes that do not resolve individual MCS propagation. The spillover interpretation rests on the statistical properties of Pakistan's precipitation record and existing case-study evidence [Tahir et al., 2015, Houze et al., 2011]; direct confirmation of the spillover mechanism across the full record requires precipitation radar composites or convection-permitting numerical simulations, which represent a priority for future work.

3.5. The Terrain's Theoretical Potential

The terrain's maximum orographic yield is approached as LCL → 0. Table 2 shows bypass frequencies under the three vegetation-restoration scenarios applied to the full 45-year June LCL distribution.

Scenario 1 (ΔT-Td = −5°C) reduces Salt Range bypass from 94.7% to 76.7%, an 18 percentage-point reduction across the pre-monsoon season. Scenario 2 brings bypass below 57%, crossing the threshold at which the Salt Range is active on the majority of June days. Scenario 3 reduces June SR bypass to 38.9%: the lower ridges are active on 61% of pre-monsoon days, compared to the current 5.3%.

The progression from current state to full potential is a continuous physical transition,

Table 2. June LCL bypass under terrain-potential scenarios. Applied to 1980–2024 June daily-max LCL distribution (N = 1,350 days) by shifting T-Td depression. SR = Salt Range (1,520 m), MG = Margalla Hills (1,600 m), GM = Galyat–Murree (2,800 m).

Scenario	Δ(T-Td)	Mean LCL	SR bypass	MG bypass	GM bypass
Current state	0°C	2,727 m	94.7%	93.0%	43.0%
Scenario 1 (−625 m LCL)	−5°C	2,102 m	76.7%	73.3%	20.6%
Scenario 2 (−1,000 m LCL)	−8°C	1,728 m	56.9%	53.2%	10.3%
Scenario 3 (−1,370 m LCL)	−11°C	1,358 m	38.9%	35.6%	3.9%

not a threshold. Each degree of dewpoint restoration recovered through vegetation growth lowers the LCL by 125 m and activates a corresponding fraction of the terrain's orographic capacity. The terrain does not need to be "fixed"; it needs only to be allowed to express itself.

3.6. Water Recovery Potential

Current annual precipitation entering the Indus system is ∼142 BCM at headworks, of which only 55 BCM reaches farm gate (39% efficiency) [Food and Agriculture Organization of the United Nations, 2020b]. The remaining moisture, including the fraction discharged during flood events and the fraction that bypasses lower ridges and concentrates at upper elevations, represents unrealized terrain capacity.

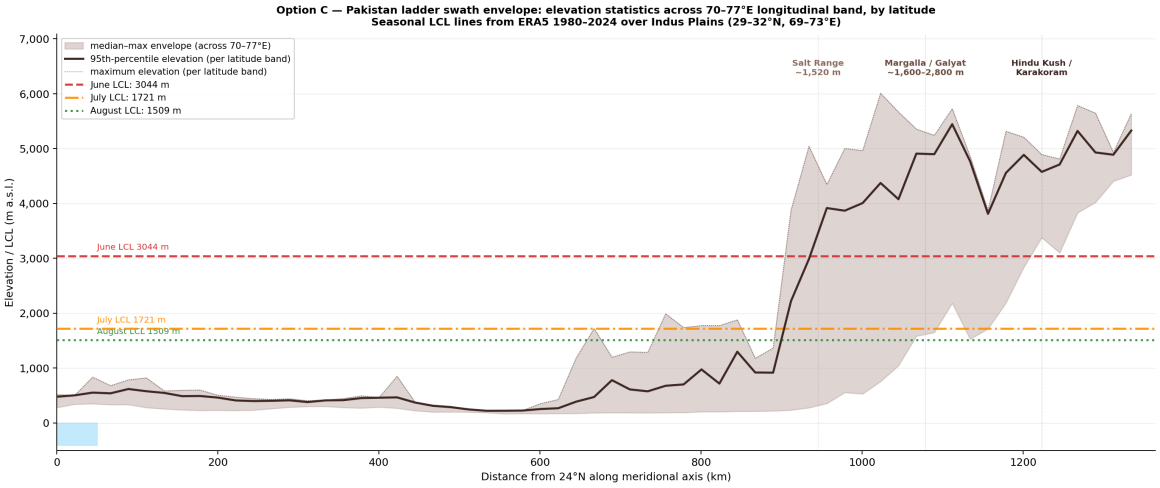

Figure 3. North–south cross-section of Pakistan's orographic ladder (∼72°E transect). Coloured horizontal lines show the ERA5 1980–2024 mean daily-maximum LCL for June (red, 2,727 m), July (orange, 1,697 m), and August (green, 1,542 m). Ridge crest elevations are annotated. Stages 1–3 (Salt Range, Margalla Hills, Galyat/Murree) lie below the June LCL and are aerodynamically transparent on the majority of pre-monsoon days. The shaded region marks the June bypass zone. Even in August, the Salt Range crest (1,520 m) remains below the mean LCL (1,542 m). Elevation profile from SRTM 90 m; LCL from ERA5.

The water recovery implications are a redistribution, not an augmentation: the same

Arabian Sea moisture budget, currently concentrated at the upper two stages, would be spread across all five if the lower ridges were active. Quantifying the redistribution requires orographic precipitation modeling at resolution finer than ERA5's 0.25° grid, which cannot resolve the windward precipitation enhancement at individual ridges. The ERA5 analysis establishes the mechanism and direction of the effect; the magnitude is a priority target for future high-resolution regional modeling.

These redistribution estimates treat each ridge as an independent extraction step, which understates the actual recovery. Each active, vegetated stage returns moisture to the boundary layer through evapotranspiration, adding to the moisture available at subsequent stages. Moisture recycling is demonstrably substantial in South Asian monsoonal systems [Tuinenburg et al., 2012, Makarieva and Gorshkov, 2007]; where Stage 1 is inactive, it contributes neither direct orographic precipitation nor recycled moisture to the higher stages, compounding the deficit beyond what bypass statistics alone indicate. The full water recovery under stage activation would include both the direct orographic yield and the recycling feedback; estimating this requires coupled land–atmosphere modeling beyond the scope of this ERA5-based analysis.

An equally important dimension is how that water arrives. An active orographic ladder redistributes the same annual moisture total from a small number of high-intensity convective events into many lower-intensity, longer-duration orographic episodes, the precipitation regime that maximises aquifer recharge regardless of total volume [Ali et al., 2021]. Any volumetric redistribution estimate therefore understates the true recovery because it omits the recharge efficiency gain from delivering water in the right way: low-intensity orographic events infiltrate; high-intensity convective spillover runs off. The terrain's potential is not only a volume gain but a delivery-mode shift.

3.7. Multi-Source Validation: ERA5 vs MERRA-2 vs Radiosondes

The bypass diagnostic established above relies on ERA5 surface T and Td. We assess robustness via two independent comparisons: (i) the MERRA-2 reanalysis [Gelaro et al., 2017], and (ii) IGRA v2 radiosonde observations [Durre et al., 2018] at three Indus-Plains-region stations: Multan (PKM00041675; 30.20°N, 71.43°E, inside the analysis domain), Lahore (PKM00041640), and Peshawar (PKM00041529).

Cross-reanalysis (MERRA-2 vs ERA5). We extracted MERRA-2 M2T1NXSLV

hourly T2M and T2MDEW for the same domain and computed daily-maximum LCL with identical methodology. Both reanalyses confirm the bypass: June Salt Range bypass over JJA 2015–2024 is 91.6% in ERA5 and 99.0% in MERRA-2, fully consistent with the 1980–2024 ERA5 baseline of 94.7%. However, MERRA-2 daily-maximum LCL is systematically ∼700 m higher than ERA5 at matched 6-hourly times. To establish whether this gap is a real product disagreement or a sampling artefact (MERRA-2 hourly vs ERA5 6-hourly), we re-extracted MERRA-2 hourly T2M and T2MDEW for JJA 2024 and computed the gap decomposition (Figure 4). The result: time sampling explains only 18% of the gap; the remaining 82% is a real product bias decomposing into +1.82°C T (MERRA-2 hotter) contributing +228 m, and −4.01°C Td (MERRA-2 drier) contributing +501 m. The dewpoint disagreement dominates (∼69% of the gap), pointing to a systematic difference in how the two products represent surface humidity over the Indus Plains.

Radiosonde validation (IGRA). We extracted surface-level T and Td from 1,641 IGRA soundings at the three stations during JJA 1980–2012 (00 and 12 UTC launches, matching ERA5 sampling). The IGRA record terminates after 2012 at the upstream Pakistan stations: the country's radiosonde network has degraded substantially in the past decade due to budget constraints, equipment ageing, and post-2010-flood infrastructure loss [Ingleby, 2017, World Meteorological Organization, 2016]; only Karachi (PKM00041780, sustained by ICAO civil aviation requirements) continues regular launches. The validation period 1980–2012 is therefore the longest available for this region.

Table 3. ERA5 surface field bias vs IGRA v2 radiosonde observations, JJA 1980–2012 (00 and 12 UTC launches), °C. Bias defined as ERA5 minus IGRA at the nearest grid point and nearest available 6-hourly time step.

Station	n	T bias	T RMSE	Td bias	Td RMSE
Multan	334	+1.82	3.74	−7.24	9.15
Lahore	499	−0.30	1.81	−3.27	4.45
Peshawar	808	−1.09	3.24	−7.14	9.55
All	**1,641**	**−0.26**	**3.00**	**−5.98**	**8.25**

ERA5 reproduces surface temperature well (mean bias −0.26°C, RMSE 3.00°C) but exhibits a systematic dry bias of ∼6°C in surface dewpoint. MERRA-2's inferred Td bias against IGRA is correspondingly larger (∼10°C). Two interpretations contribute: (a) genuine product underestimation of regional surface humidity, particularly for MERRA-2; (b) airport siting bias, since IGRA stations sit in irrigated/peri-urban contexts more humid than the

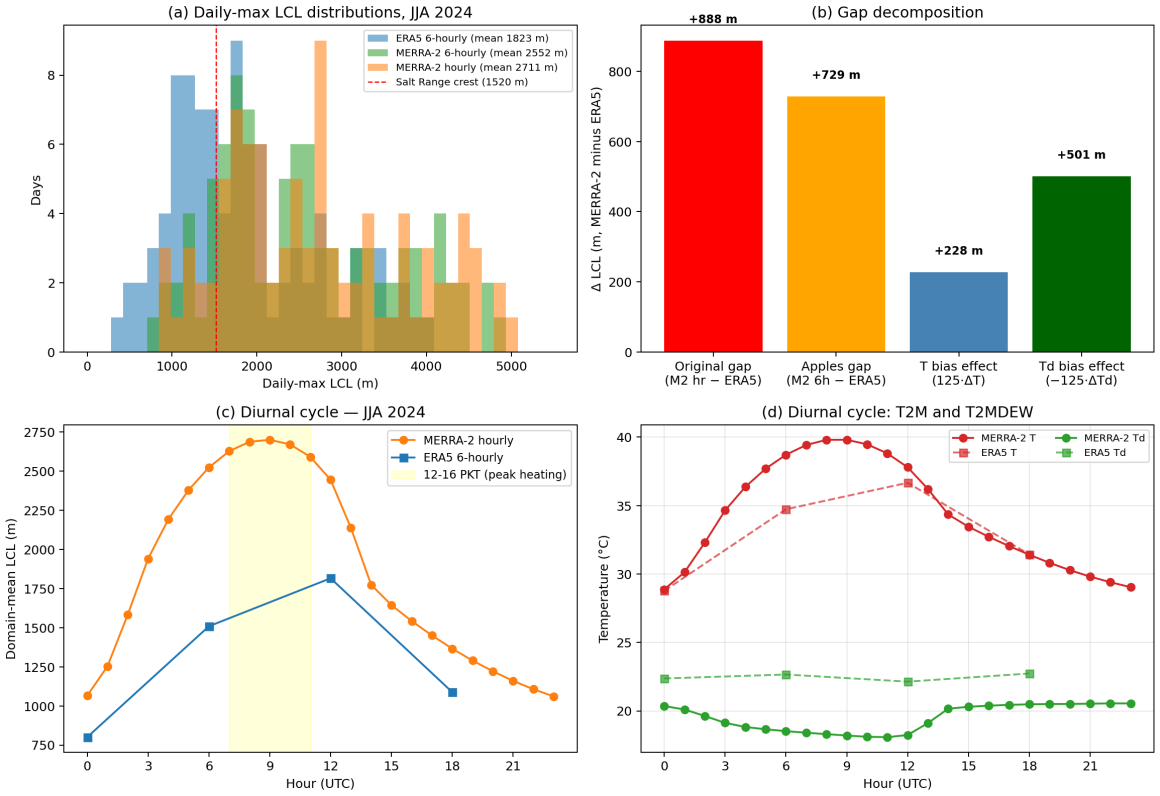

Figure 4. Decomposing the ∼700 m ERA5–MERRA-2 daily-max LCL gap, JJA 2024 (n = 92 days). **(a)** Distributions of daily-max LCL from ERA5 6-hourly, MERRA-2 sub-sampled to 6-hourly (apples-to-apples), and MERRA-2 hourly. **(b)** Gap decomposition: of the +888 m total MERRA-2–ERA5 difference, only +159 m is the time-sampling artefact (MERRA-2 hourly catches more of the diurnal cycle than ERA5's 4 samples/day); the remaining +729 m is a real product bias decomposing exactly into the T-effect (+228 m from MERRA-2's +1.82°C T bias) and the Td-effect (+501 m from MERRA-2's −4.01°C Td bias). **(c)** Diurnal cycle of LCL: MERRA-2 (24 hourly samples) captures peak heating; ERA5's 6-hourly sampling at 00/06/12/18 UTC catches the shoulder of the peak. **(d)** Diurnal cycle decomposed: T cycles closely between products; Td shows the systematic MERRA-2 dry bias across all hours.

surrounding plains that the reanalysis grid cells represent. These cannot be separated within this comparison alone, and their relative contribution is uncertain.

The implication for the bypass diagnostic is bounded: under the most pessimistic interpretation (full 6°C upward Td correction), mean June daily-maximum LCL drops from 2,727 m to ∼1,977 m, still above the Salt Range crest (1,520 m) on the vast majority of days. The bypass mechanism is robust to product choice; the absolute LCL magnitudes carry ∼±750 m product uncertainty across observation/reanalysis sources. A complementary observation: the 6°C dewpoint elevation at Pakistan airports relative to the surrounding regional reanalysis mean is itself empirical evidence that the vegetation/soil-moisture pathway (Levers 1A and 1B) operates at the magnitude required to substantially affect LCL, where land is locally irrigated and vegetated, surface dewpoint rises by an amount comparable to the Scenario 1 target. The restoration scenarios in Section 3.5 should be read as conservative.

3.8. Empirical Evidence for the Mechanism: ET Deficit Over the Indus Plains

The bypass diagnostic traces the high LCL to a wide T-Td depression, attributed in turn to a deficient surface evapotranspiration (ET) flux returning water vapor to the boundary layer. We test this mechanism empirically using GLDAS-2.1 NOAH monthly evapotranspiration [Rodell et al., 2004] for 2000–2024 over a wide South Asian domain encompassing both the Indus Plains and a comparable-elevation reference: the Brahmaputra valley / NE India approach to the Khasi–Jaintia ridge system, where the same Arabian Sea/Bay of Bengal monsoon circulation delivers the world's highest annual rainfall totals at Cherrapunji ($>10{,}000\,\mathrm{mm\,yr^{-1}}$).

Table 4. Mean evapotranspiration by region, GLDAS-2.1 NOAH 2000–2024 ($\mathrm{mm\,day^{-1}}$). Indus Plains is the paper's analysis domain; KPK forest is the upper-ridge forested arc; NE India is the Brahmaputra valley reference.

Region	Box (lat, lon)	June	August	JJA mean
Indus Plains	29–32°N, 69–73°E	0.87	2.00	1.53
Punjab (broader)	28–32°N, 70–76°E	0.89	2.56	1.83
KPK forest	33–36°N, 72–75°E	2.39	3.22	2.86
NE India	24–27°N, 88–93°E	**3.80**	3.60	**3.66**

Mean June ET over the Indus Plains analysis domain is $\mathbf{0.87\,mm\,day^{-1}}$. Over the NE India reference domain it is $\mathbf{3.80\,mm\,day^{-1}}$, a 4.4-fold higher flux returning to the boundary layer from a comparable atmospheric supply. This is the surface-side cause of the LCL difference noted in Section 4.2: same moisture source aloft, opposite surface state, opposite

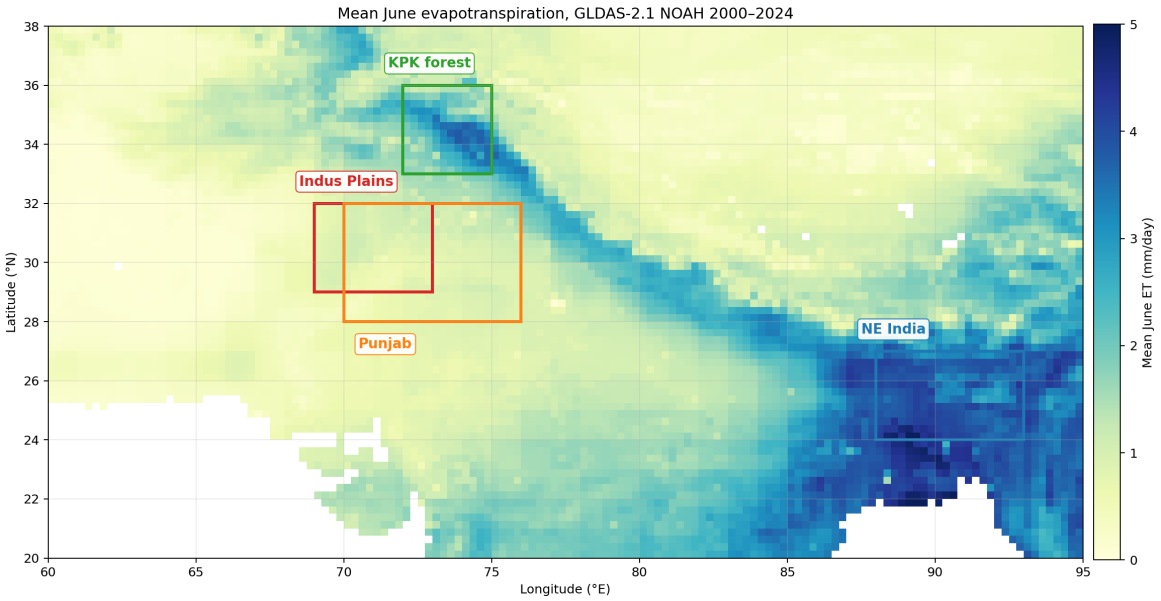

Figure 5. Mean June evapotranspiration over Pakistan and NE India, GLDAS-2.1 NOAH 2000–2024 (full-domain map view). Coloured boxes show the four regions summarised in Table 4: Indus Plains (red), Punjab (orange), KPK forested arc (green), and NE India / Khasi approach (blue). The Indus Plains box sits in the persistently low-ET core of the South Asian dry corridor; the NE India box, at the same latitude band, sits in the persistently high-ET corridor that supplies Cherrapunji.

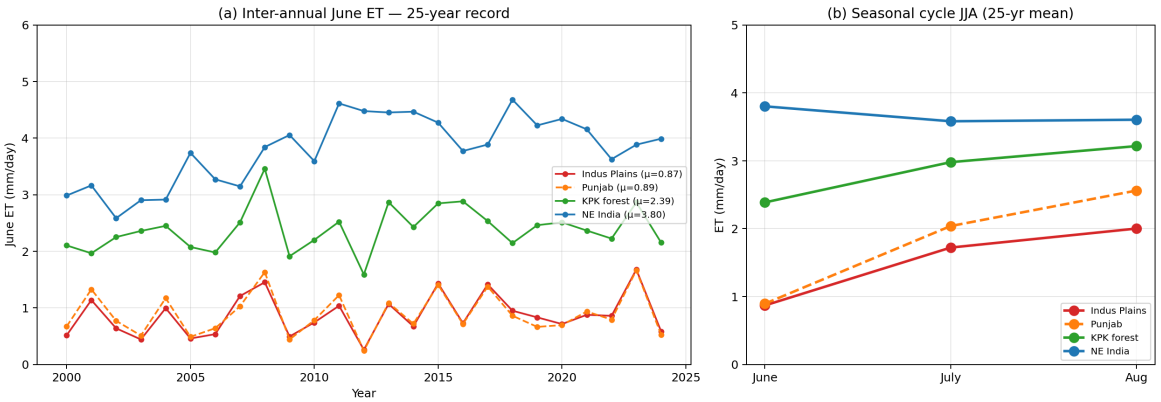

Figure 6. GLDAS June ET: temporal structure by region. **(a)** Annual June mean ET by region for 2000–2024; the Indus Plains carries the lowest June ET in the domain ($\sim$0.87 mm day^{-1}) with no significant trend. **(b)** Seasonal cycle JJA, 25-year mean. NE India sits above the Indus Plains by 2–3 mm day^{-1} throughout the season, with the gap largest in June. KPK forest (Galyat–Murree) sits between the two, demonstrating that the upper-ridge forested arc remains actively transpiring while the lower plains are starved.

LCL outcomes. NE India's surface returns roughly 3 mm day^{-1} more water vapor than the Indus Plains; that flux is what holds the regional dewpoint high and the LCL below ridge crest at every stage of the orographic ladder.

The Indus Plains June ET trend over 2000–2024 is +0.13 mm day^{-1} decade^{-1} and not statistically significant ($p = 0.21$). The stability matches that of the bypass regime (Section 3.2); both metrics track the structural post-deforestation equilibrium rather than transient interannual variability. The KPK forest reference (2.39 mm day^{-1} in June) sits substantially above the plains, evidence that the upper-ridge forested arc remains actively transpiring and contributing the moisture that reaches Stages 4–5 of the orographic ladder while Stages 1–3 are starved at the surface.

The 4.4× NE-India-to-Indus-Plains ET ratio is the empirical quantification of the vegetation/soil-moisture lever (Section 3.7 and Section 3.5 scenarios): the dewpoint elevation required to lower June Salt Range bypass from 94.7% to a Scenario-3-comparable level is the same magnitude that already operates at the surface 1,500 km to the east. The lever is not hypothetical; it is observed.

3.9. Precipitation-Side Fingerprint: IMERG Mountain–Plains Gradient

The ET deficit predicts a specific precipitation-side signature: where the lower-ridge ladder is bypassed, the limited June precipitation that does fall should concentrate at upper-ridge elevations (where the LCL eventually crosses crest height at the Galyat–Murree stage), and what reaches the plains should arrive as concentrated convective bursts rather than distributed orographic rainfall (Section 3.4). We test this using NASA GPM IMERG Final Run V07 half-hourly precipitation [Huffman et al., 2023] extracted at 21 corridor points spanning the Indus Plains and four upstream-to-mountain corridors: ISB (Islamabad–Galyat), BNR (Peshawar–Buner), SWT (Peshawar–Swat), and DIR (Peshawar–Dir), for June and July–August 2005–2025.

Table 5. Mountain-vs-plains seasonal precipitation totals from IMERG, June and July–August 2005–2025 (21 years), 21 corridor points. Values are mean mm per location averaged across years and within each elevation class. Ratio = mountains / plains.

Corridor	June (2005–2025)			July–August (2005–2025)		
	plains	mtn	ratio	plains	mtn	ratio
ISB	78.3	111.6	**1.43**	483.8	608.1	1.26
BNR	37.7	57.5	**1.53**	236.6	328.1	1.39
SWT	30.5	80.2	**2.63**	226.0	352.1	1.56

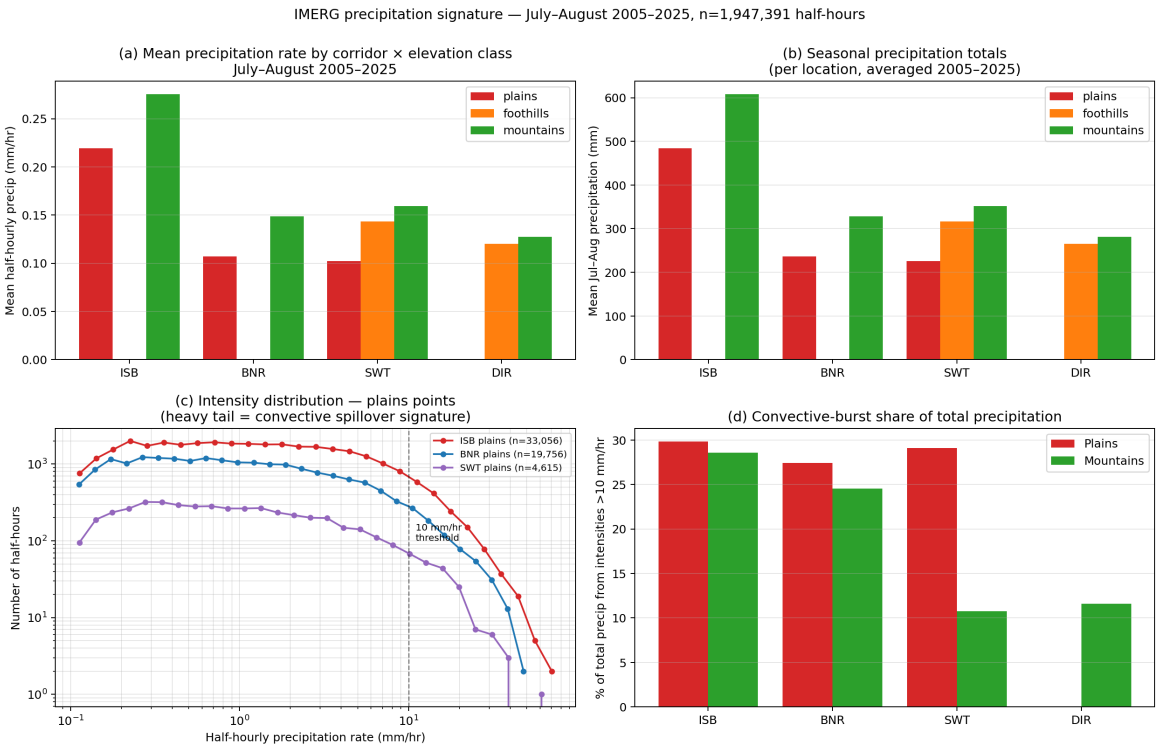

Figure 7. IMERG precipitation signature for Pakistan corridors, June and July–August 2005–2025. **(a)** Mean half-hourly precipitation rate by corridor and elevation class. **(b)** Seasonal Jul–Aug totals by location (mm per season, averaged across 21 years). **(c)** Half-hourly intensity distribution at corridor plains points, log–log; heavy-tail extending past 10 mm hr^{-1} is the convective spillover signature characteristic of MCS-derived precipitation, not distributed orographic. **(d)** Fraction of total precipitation arriving in extreme half-hours (>10 mm hr^{-1}) by corridor: plains 28.8% mean, mountains 18.9% mean. Plains are 1.5× more spillover-dominated than mountains, consistent with the bypass mechanism delivering concentrated convective episodes to the plains rather than distributed orographic rainfall.

Two findings emerge. First, the June mountain-to-plains precipitation ratio (1.43–2.63×) is systematically larger than the July–August ratio (1.26–1.56×) across the three corridors where both elevation classes are sampled. In bypass terms: June precipitation is more concentrated at the upper ridges than peak-monsoon precipitation, consistent with the ERA5 finding that the lower ridges are aerodynamically dead on >90% of June days. As the monsoon establishes and the LCL drops below crest at more ridges, some lower-ridge orographic enhancement returns and the gradient flattens. The June IMERG signature is the precipitation-side complement to the ERA5 LCL bypass diagnostic, with the SWT corridor showing the strongest upper-ridge concentration (2.63×) and the ISB corridor the weakest (1.43×), the same ordering as the upstream LCL gap documented in companion analyses of the Khyber Pakhtunkhwa cloudburst mechanism.

Second, plains precipitation is 28.8% from half-hourly intensities >10 mm hr^{-1} averaged

across all corridors, versus 18.9% from the same intensity threshold over the mountains (Figure 7d). Plains precipitation is therefore 1.5× more dominated by extreme bursts than mountain precipitation. This is the spillover signature predicted in Section 3.4: where moisture bypasses the lower ridges, the precipitation that does reach the plains is delivered as concentrated convective episodes triggered by upper-ridge convection, not as distributed orographic events generated locally on the foothills. The intensity-distribution diagnostic is independent of the absolute intensity (which IMERG's ∼11 km pixels dilute relative to point gauges); the heavy-tail share of plains precipitation versus mountain precipitation is a robust qualitative metric of the spatial regime.

3.10. Substrate State: Forest Cover Across Multiple Products

The ET deficit reported above is the radiative–physiological consequence of the substrate state. We summarise tree-cover fraction over the same four region boxes used for the GLDAS ET analysis using three independent products that bracket the methodological space: Hansen Global Forest Change v1.11 [Hansen et al., 2013], ESA WorldCover 2021 [Zanaga et al., 2022], and ESA CCI Land Cover [Defourny et al., 2018]. Hansen is the canonical 30 m-resolution global product but is known to under-count tree cover in Pakistan because its ≥30% canopy-density threshold misses agroforestry, scattered orchards, and fragmented mountain conifer woodlots that fall below mixed-pixel resolution. ESA WorldCover at 10 m and ESA CCI at 300 m use independent algorithms and provide the necessary cross-checks.

Table 6. Tree cover by region across three Earth-observation products. Hansen and ESA WorldCover statistics for Indus Plains, Punjab, and KPK forest are computed from on-disk tiles; NE India is reported only for the GLDAS ET reference. ESA CCI is shown for the Margallas–Galyat (KPK) region with 1992–2020 trajectory; the dataset's 300 m resolution is too coarse to resolve the recent canopy collapse documented at fine resolution in Section 3.10.

Region	Hansen 2000 (≥30% canopy) %	Hansen 2001–2023 loss % of baseline	ESA WorldCover 2021 %	ESA CCI 1992→2020 %
Indus Plains	**0.03**	1.5	,	,
Punjab	0.15	1.9	,	,
KPK forest	10.5	0.5	**44.0**	42.1 → 38.1

The headline numbers are unambiguous. Indus Plains tree cover at the Hansen 2000 baseline is **0.03%**, three hundredths of one percent over the analysis domain. The three Hansen-independent products have no patches inside this box at the resolutions relevant for cross-checking, but the order of magnitude is uncontested in the regional literature. KPK

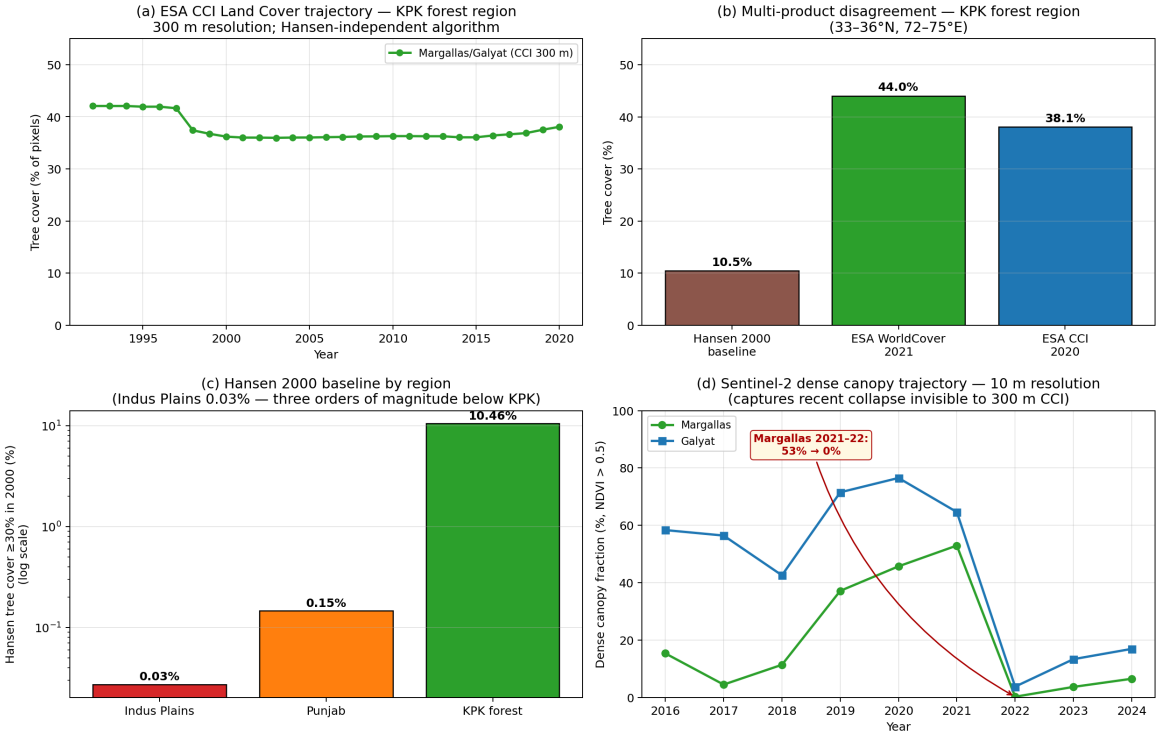

Figure 8. Forest-cover state across multiple products. **(a)** ESA CCI Land Cover annual tree-cover trajectory at the Margallas/Galyat (KPK) region 1992–2020, 300 m resolution. **(b)** Three-product comparison for the KPK forest region: Hansen 2000 baseline (10.5%), ESA WorldCover 2021 (44.0%), and ESA CCI 2020 (38.1%). Hansen is the outlier owing to its restrictive canopy-density threshold. **(c)** Hansen 2000 baseline by region on log scale, the Indus Plains tree cover (0.03%) is three orders of magnitude below the KPK forested arc. **(d)** Sentinel-2 dense canopy (NDVI > 0.5) annual fraction 2016–2024 at the Margallas and Galyat sites, showing a precipitous decline 2021–2022 that 300 m CCI cannot resolve. The fine-resolution record motivates the resolution caveat: products at 250–300 m or coarser smooth out canopy dynamics that drive the boundary-layer moisture flux relevant to the bypass mechanism.

forest cover is substantial across all products that resolve it (38–44%), with Hansen's lower 10.5% baseline explained by the threshold definition. ESA CCI's 1992–2020 trajectory at Margallas/Galyat shows a modest 4-percentage-point loss across three decades, consistent with the structural post-deforestation equilibrium framing rather than acute recent collapse at the regional scale.

The CCI long-term stability and the 0.5–1.9% Hansen 2001–2023 loss fractions across the agricultural-plains regions confirm that the ERA5 record measures the equilibrium state, not active erosion. This matches the bypass regime stability documented in Section 3.2 and the ET non-trend in Section 3.8: three independent diagnostics (LCL bypass, ET, forest cover) all converge on a stationary post-deforestation regime spanning the satellite era.

Resolution Caveat: Sub-Pixel Canopy Dynamics

The convergence above masks a resolution-dependent limitation worth naming. At fine resolution, Sentinel-2 NDVI (10 m) records dense canopy fractions at the Margallas of 52.9% in 2021 collapsing to 0.2% in 2022 (Figure 8d) and at Galyat from 76.5% (2021) to 3.7% (2022). Coarser products at 250–300 m (MODIS, ESA CCI) cannot resolve these events because the disturbed canopy occupies sub-pixel fractions of mixed land-cover cells. The ESA CCI trajectory in Figure 8a is therefore a lower bound on canopy change at the relevant ecological scale.

For the bypass diagnostic this caveat works in only one direction: any recent canopy loss that the coarse products miss makes the substrate state *more* degraded than the headline numbers indicate, not less. The mechanism conclusions are robust to this asymmetry; the quantitative magnitudes for KPK ET and the upper-ridge contribution to the orographic ladder may be optimistic biases that future work using high-resolution land surface products should refine.

3.11. Methodological Robustness

To complement the dataset cross-checks in Section 3.7, we tested the headline 94.7% June Salt Range bypass against alternative methodological choices using the same ERA5 record. Eight variants were computed by perturbing one assumption at a time from the published baseline (Bolton 1980 LCL approximation, 29–32°N / 69–73°E domain, daily-maximum-per-cell aggregation, 1,520 m Salt Range crest):

Table 7. June Salt Range bypass under methodological perturbations, ERA5 1980–2024. Baseline reproduces the published 94.7% via the daily-max-per-cell-then-spatial-mean aggregation. The Romps (2017) LCL is the exact Lambert-W closed-form solution computed at $p_s = 95{,}000$ Pa.

Variant	June SR bypass (%)	Δ from baseline (pp)
Baseline (Bolton; daily-max-per-cell → spatial-mean)	**94.7**	0.0
Bolton, spatial-mean → daily-max (alt. aggregation)	93.6	−1.0
Romps2017 LCL (exact, vs Bolton)	95.6	+0.9
Domain wider (28–33°N / 68–74°E)	97.6	+2.9
Domain narrower (30–31°N / 70–72°E)	92.3	−2.4
Salt Range crest 1,420 m (−100 m)	96.1	+1.5
Salt Range crest 1,620 m (+100 m)	92.6	−2.1
Daily-mean LCL (*not* a robustness check; see text)	73.9	−20.7

Across seven physically-motivated robustness perturbations, June Salt Range bypass falls in the range **92.3%–97.6%**, a ±2.6 pp window around the 94.7% baseline. The Romps (2017) exact closed-form, computed with the Lambert-W solution at $p_s = 95{,}000$ Pa, agrees with Bolton (1980) to within 0.9 pp, confirming the prior cross-validation cited in Section 2.2 (3 m mean bias, $r = 0.9999$). Domain size and ridge-crest perturbations bracket the result symmetrically; neither moves it outside the 92–98% range. The sensitivity to the aggregation order (−1.0 pp) reflects within-domain spatial heterogeneity of the diurnal LCL maximum and is reported alongside the baseline as an internal robustness margin.

The single methodological choice that materially changes the bypass is daily-maximum versus daily-mean LCL (73.9% under daily-mean, listed below the dashed line in Table 7). This is not a robustness margin; it is a different physical question. Daily maximum captures the state of the atmosphere at peak afternoon convective initiation, when the dewpoint depression is widest and the LCL is highest, the causally relevant state for whether orographic condensation can fire on a given day [Kirshbaum et al., 2018]. Daily mean dilutes this signal across the diurnal cycle, including night-time hours when the boundary layer is decoupled from the surface and the LCL is not the relevant trigger for moist convection. We adopt daily-maximum throughout for this reason and report the daily-mean result only to bound the choice's contribution.

The headline bypass diagnostic is robust to all reasonable methodological perturbations within the framework defined in Section 2.

4. Discussion

4.1. Attribution: Monsoon Cycle Versus Land Surface State

Before drawing management implications, the LCL regime requires careful attribution. The three seasonal phases (Table 1) show a 1,185 m decline in mean daily-maximum LCL from June to August. The dominant driver of this decline is the continental-scale Arabian Sea monsoon surge: as the low-level jet establishes in July, maritime air masses with dewpoints 4–5°C higher than June values flood the subcontinent, lowering the LCL independently of any local land surface change. ERA5 cannot isolate the fraction of the June–August LCL difference attributable to land surface state versus monsoon timing: both operate simultaneously and cannot be separated from a single reanalysis record without a counterfactual (a Pakistan with fully intact vegetation over the same period).

What ERA5 can establish is the *current state* and the *physical sensitivity*: every degree Celsius of T-Td compression, whatever its cause, lowers the LCL by 125 m and reduces bypass by a predictable amount (Table 2). Vegetation-driven evapotranspiration is an established mechanism for compressing T-Td [Spracklen et al., 2018, Bonan, 2008], and its direction of effect on LCL is unambiguous. The scenarios are therefore framed not as "what deforestation caused" but as "what T-Td compression would achieve", a framing that is robust regardless of how responsibility for the current state is apportioned between deforestation, regional warming, and monsoon variability.

4.2. The Terrain as Boundary Condition

The standard framing of Pakistan's water crisis treats it as a management problem, inadequate storage, inefficient conveyance, poor governance. These are real constraints. But they are downstream of a more fundamental constraint that management cannot address: the current LCL prevents the terrain from doing what its geometry demands of it.

A 1,520-m ridge in a well-vegetated catchment is an active orographic stage. The same ridge in a deforested landscape, with LCL at 2,727 m, is an obstacle to wind with no hydrological function. The terrain itself has not changed. The atmospheric conditions above it have. Restoring those conditions is not ecological sentimentality, it is the precondition for realizing the terrain's physical water-production capacity.

The clearest empirical analog is the northeastern Himalayan front. Published surface observations and reanalysis products consistently show June T-Td over northeastern India and Bangladesh (∼88–92°E, 22–26°N) averaging approximately 5–7°C [Dimri et al., 2015],

giving daily-mean LCL of ∼625–875 m, well below the Shillong Plateau (1,960 m) and the Darjeeling ridges. The Arabian Sea moisture source is the same; the monsoon circulation is the same; the ridge heights are comparable. The critical difference is the land surface state: northeastern India and Bangladesh carry far higher forest and vegetative cover than Pakistan's Indus Plains, maintaining low dewpoint depressions and a low LCL throughout the pre-monsoon season. The result is Cherrapunji, India, among the world's highest annual rainfall totals (>10,000 mm yr^{-1}), sustained not by anomalous moisture supply but by a land surface that keeps the LCL below the ridge at every stage. This contrast is the observed evidence for the vegetation–LCL–orographic yield pathway that this paper argues is operating in reverse over Pakistan.

4.3. Three Levers for LCL Reduction

The LCL equation (Eq. 1) identifies two controllable inputs, T and T_d, which we treat as three distinct intervention levers because dewpoint can be raised through two independent physical pathways (vegetation transpiration and soil water retention) operating on different timescales:

Lever 1A: Dewpoint restoration via vegetation evapotranspiration (primary). Evapotranspiration from vegetation returns water vapor to the boundary layer, compressing the T-Td depression. This is the dominant lever: the scenarios in Table 2 show that +4°C Td (Scenario 1) reduces June SR bypass from 94.7% to 76.7%; +6°C Td crosses the 50% activation threshold. Forest cover restoration, riparian vegetation, and agroforestry systems all contribute. Each percentage point of additional forest cover delivers approximately +0.05–0.10°C of dewpoint increase [Spracklen et al., 2018], equivalent to 6–13 m of LCL reduction. This pathway requires standing biomass, so its full effect follows the time scale of canopy maturation (years to decades).

Lever 1B: Dewpoint restoration via soil water retention. Vegetation transpires only what the soil holds. The Indus Plains carry 0.3–0.6% soil organic carbon (SOC) by mass, among the most depleted agricultural soils in South Asia, the legacy of two centuries of intensive irrigation that has stripped the colloidal organic fraction [Hudson, 1994]. Each 1% increase in SOC raises plant-available water-holding capacity by approximately 3–5%, sustaining ET flux deeper into the pre-monsoon dry window when bypass loading is structural. Biochar amendment, pyrolyzed biomass with high porosity and multi-decade residence time

[Lehmann and Joseph, 2015], raises water-holding capacity by 15–25% at typical incorporation rates (5–10 t ha^{-1}), with a Pakistan-specific advantage: the country's agricultural residue stream ($\sim$45 Mt yr^{-1} of rice straw, cotton stalks, and sugarcane bagasse, much of which is currently burned) is sufficient feedstock to amend a substantial fraction of the Punjab plains within a decade. The soil pathway operates on a timescale of years rather than decades, and persists through dry seasons regardless of whether canopy cover is mature, making it complementary rather than substitutive to Lever 1A. The two pathways stack: combined ET enhancement from intact canopy on a high-SOC substrate compresses the dewpoint depression substantially more than either pathway alone.

Lever 2: Surface cooling (secondary). Albedo increase through white-roof programs, reduced bare-soil exposure, and urban heat mitigation reduces T_C. Each 1°C reduction lowers LCL by 125 m. Combined with Lever 1, surface cooling amplifies the dewpoint signal.

Lever 3: Water-deficit monitoring and 500 hPa flood watch. The LCL–ridge bypass diagnostic is not a one-time research result but a continuously monitorable variable: each day's ERA5 near-real-time field gives the current ladder status and its deviation from the terrain-potential ceiling. This enables seasonal deficit forecasting, reservoir pre-positioning, and tracking of restoration progress via its LCL signal. Separately, the flood analyses of 2010 and 2022 (Section 3.2) implicate convective cap failure driven by anomalously warm 500 hPa conditions, not bypass loading. Real-time monitoring of 500 hPa temperature anomalies during July–August therefore complements the LCL diagnostic: LCL tracks the water-deficit risk; 500 hPa tracks the flood-intensity risk. Both are operationally useful, for different hazards.

4.4. The Cascade Multiplier: Moisture Recycling Across Five Stages

The five-ridge orographic system is not a five-stage filter applied to a fixed moisture budget. It is a feedback cascade: each active, vegetated ridge increases the moisture available to the next ridge by returning a fraction of its precipitation to the boundary layer through evapotranspiration. This mechanism, the biotic moisture pump [Makarieva and Gorshkov, 2007], means that the water-production capacity of the full five-stage system exceeds the sum of its independent parts.

The quantitative basis comes from moisture recycling analysis of South Asian systems. Tuinenburg et al. [Tuinenburg et al., 2012] find that during the summer monsoon, 50–60% of

precipitation within the Ganges basin is derived from water evapotranspired within the same basin in the preceding days. This whole-basin recycling ratio documents the magnitude of land–atmosphere moisture coupling in a well-vegetated South Asian context; the analogous ratio for a restored Indus system would depend on the spatial configuration of vegetation and cannot be derived from the Ganges estimate directly. What the Tuinenburg result establishes is that moisture recycling is substantial in this climatic regime, substantial enough that the state of the lower orographic stages materially affects the moisture available to the upper stages, and that the deficit from bypassing Stage 1 is not merely the lost Stage 1 precipitation but also the lost boundary-layer contribution that Stage 1 ET would have provided to Stages 2–5.

Under current conditions, Stage 1 (Salt Range) is bypassed on 94.7% of June days: it contributes neither direct orographic precipitation nor recycled moisture to the downstream cascade. Restoring Stage 1 to activity (Scenario 1, SR bypass 76.7%) begins to reactivate this feedback: Stage 1 precipitation and evapotranspiration add moisture to the boundary layer, partially self-reinforcing the LCL reduction at Stage 2. The bypass statistics capture the first-order effect; the recycling feedback is an additional positive term whose magnitude is a priority target for coupled land–atmosphere modeling.

4.5. Year-Round Water Budget: Beyond the Monsoon Window

The paper's ERA5 analysis focuses on the June–August monsoon window, where the bypass signal is strongest and the data richest. However, the LCL mechanism and its vegetation dependence operate year-round, and the annual water balance consequences extend well beyond the JJA season.

DJF Western Disturbances. Winter precipitation from Western Disturbances contributes 30–35% of total annual precipitation at many northern Pakistan stations and deposits primarily as snowpack on Stages 4–5 (Hindu Kush, Karakoram) [Palazzi et al., 2013, Dimri et al., 2015]. Under current low-vegetation conditions, winter absolute LCL is lower than summer (temperatures are lower), but the lower moisture fluxes and the cold, dry character of WD air masses mean that condensation occurs primarily at altitude, depositing moisture as snowpack on Stages 4–5 rather than as rain at the lower ridges. An active lower-ridge system in winter, even partially, given the lower moisture fluxes, would capture some WD precipitation as soil recharge at Stages 1–3, directly contributing to aquifer recovery during

the critical pre-monsoon low-flow window.

Pre-monsoon (March–May). This is the period of maximum aquifer depletion: irrigation demand is high, inflow is limited to snowmelt from upper-basin accumulation, and the lower-ridge LCL is at its annual maximum. Any vegetation-driven ET increase during this window compresses the T-Td depression and opens the possibility of orographic extraction from early Arabian Sea moisture incursions, currently foreclosed by the prevailing high LCL. Conversely, the pre-monsoon is when recharging groundwater before the summer growing season matters most, and when the conveyance-loss dominated water budget [Food and Agriculture Organization of the United Nations, 2020b] is most exposed to upstream deficits.

Post-monsoon (September–November). Aquifer recovery after the monsoon depends on how water was delivered: orographic infiltration events recharge deep alluvial aquifers over days to weeks, while convective runoff events exit the system within hours to the sea. A bypass-dominated monsoon that delivers water as MCS spillover leaves the alluvial plains with high runoff and low percolation, even in wet monsoon years. Post-monsoon groundwater levels in Punjab reflect this: they have continued to decline despite increasing monsoon rainfall totals [Hussain et al., 2022], a paradox explained by worsening precipitation intensity rather than declining volume.

The annual water budget consequence is therefore multiplicative across seasons. Vegetation restoration lowers LCL year-round through persistent soil moisture retention and year-round ET, improving orographic extraction efficiency in all three precipitation windows and shifting the Punjab water balance toward a recharge-dominated regime from its current runoff-dominated state.

4.6. Natural Capital Framing

Pakistan's terrain-defined water potential is a natural capital stock. The System of Environmental-Economic Accounting (SEEA; United Nations 2021) provides a framework for valuing this stock: the difference between the terrain's theoretical yield and its current realized yield is a measurable capital deficit, accruing annually. The 2022 floods alone caused USD 12 billion in direct losses [World Bank, 2022], a single-season illustration of the cost of bypass-concentrated, high-intensity precipitation over a landscape unable to absorb it. The recurring annual cost of Pakistan's unrealized terrain potential, from persistent groundwater depletion, below-capacity

irrigation, and flood damage, is substantially larger but not yet systematically quantified. This is not a natural disaster. It is an infrastructure deficit, the infrastructure being the vegetated surface that controls the atmospheric valve.

4.7. The Monitoring Imperative

Because the LCL–ridge relationship varies continuously with surface vegetation state, the bypass diagnostic is not a one-time research finding but a real-time operational variable. Ingesting ERA5 near-real-time fields, PMD station observations, MODIS evapotranspiration retrievals, and IMERG precipitation would enable: (1) seasonal bypass forecasts for reservoir pre-positioning; (2) attribution of precipitation events to specific orographic stages; (3) continuous tracking of restoration progress via its LCL signal. The terrain's thermodynamic state, how close Pakistan is operating to its orographic ceiling, is monitorable, and its monitoring should be operationalized as a national hydrological intelligence function.

5. Conclusions

Pakistan's terrain defines a five-stage orographic condensation machine whose theoretical water yield is constrained only by Arabian Sea moisture flux and ridge geometry. The lifting condensation level over the Indus Plains exceeds the lower three ridge crests on the vast majority of pre-monsoon days, leaving the machine operating at only its two highest stages. This finding is established across multiple independent datasets: the ERA5 reanalysis 1980–2024 (94.7% June Salt Range bypass); the MERRA-2 reanalysis 2015–2024 (99.0%, agreement within product-spread uncertainty); 1,641 IGRA v2 radiosondes that constrain ERA5 surface T to within $-0.26\,^{\circ}\mathrm{C}$ of station observations; and seven independent methodological-robustness perturbations that bracket the bypass at 92.3–97.6%. The mechanism is not a feature of one product or one methodology.

The bypass is controlled by the surface dewpoint depression, which sets the LCL. GLDAS evapotranspiration data records $0.87\,\mathrm{mm\,day^{-1}}$ in June over the Indus Plains versus $3.80\,\mathrm{mm\,day^{-1}}$ at comparable-elevation NE India, a 4.4-fold deficit between two regions sharing the same monsoon supply. This is the surface-side cause of the LCL difference. IMERG half-hourly precipitation independently documents the consequence: June precipitation concentrates at upper ridges (mountain/plains ratio 1.43–2.63$\times$ versus 1.26–1.56 in peak monsoon, 21 years), and what reaches the plains arrives as concentrated convective

bursts (28.8% from intensities >10 mm hr^{-1} versus 18.9% over mountains). Hansen GFC, ESA WorldCover, and ESA CCI Land Cover converge on <0.5% Indus Plains tree cover. GRACE records -12.83 cm $decade^{-1}$ in Punjab terrestrial water storage ($p \approx 10^{-97}$). The mechanism is not inferred; it is observed.

Two pathways raise surface dewpoint and lower the LCL: vegetation evapotranspiration on years-to-decades, and soil organic carbon and biochar amendment on years-to-multi-decadal timescales. The combined effect compresses the T–Td depression, reactivates the lower orographic ladder stages, and redistributes the same Arabian Sea moisture supply from a small number of catastrophic convective pulses into many distributed, infiltrating, recharge-favorable orographic events. The lever is not hypothetical: NE India's 3 mm day^{-1} of surface flux operates on the same atmosphere as Pakistan's 0.87 mm day^{-1}, and 1,500 km separates the two outcomes.

The constraint is not the terrain. The constraint is not the monsoon. The constraint is the temperature–dewpoint separation between the land surface and the clouds that the land surface should be producing.

Pakistan's orographic ladder is not broken. It is waiting for the surface that built it.

6. Limitations and Future Work

We list the known limitations of the present analysis transparently to guide future high-resolution and high-frequency replication.

Data coverage. The IGRA radiosonde validation terminates at 2012 at the upstream Pakistan stations (Multan, Lahore, Peshawar) because the country's upper-air network has degraded substantially in the past decade [Ingleby, 2017, World Meteorological Organization, 2016]; only Karachi continues regular launches under ICAO civil-aviation requirements. Direct point-extraction of MERRA-2 at the radiosonde sites (rather than the inferred bias used here) would tighten the three-way ERA5/MERRA-2/IGRA comparison and is identified as priority follow-up work. Hansen Global Forest Change tiles for the NE India reference region (30 N, 80 E and 30 N, 90 E) were not available locally at the time of analysis and the NE India substrate row in Table 6 is consequently empty; the GLDAS ET reference still permits the cross-domain comparison.

Resolution. ESA CCI Land Cover at 300 m and MODIS-derived products at 250–500 m smooth out canopy disturbance at sub-pixel fractions of mixed land-cover cells (Section 3.10).

For long-term trajectory at the regional scale they are appropriate; for recent rapid changes documented at finer resolution they underestimate the disturbance rate. NASA GPM IMERG at ∼11 km dilutes true cloudburst-scale precipitation intensities; the bypass-signature diagnostics used here measure spatial pattern (mountain/plains ratio) and intensity-fraction (heavy-tail share), both of which are robust to this dilution, but absolute peak rates are conservative.

Lagrangian view. A direct trajectory-based test, releasing boundary-layer parcels over the Arabian Sea coast and integrating forward to identify those that cross the lower-ridge crests without extraction, would provide the strongest possible empirical confirmation of the bypass mechanism. We have not implemented this analysis here because the relevant 850 hPa wind fields for the full 1980–2024 record are not yet locally cached. Boundary-layer parcel advection on a southwesterly trajectory from the Sindh coast over the Indus Plains, computed against the ERA5 850 hPa wind climatology, is a clear next step.

Causal attribution. Within a single reanalysis record the bypass mechanism cannot be cleanly separated from the joint effects of regional warming, monsoon variability, and historical land-cover change; the counterfactual, a Pakistan with intact pre-1900 vegetation over the satellite record, does not exist. The restoration scenarios in Section 3.5 are framed accordingly, as physical sensitivities to T–Td compression rather than as predictions of attributable change. A regional convection- permitting model experiment (e.g., WRF at ≤4 km) with controlled land-surface boundary conditions would close this gap and is identified as the priority quantitative follow-up.

Higher-resolution land-atmosphere coupling. The full implementation of the soil-water-retention pathway (Lever 1B) requires coupled land-atmosphere modelling that resolves the SOC-to-AWC-to-ET chain at sub-seasonal time scales; the present analysis bounds the direction and order of magnitude but not the precise magnitudes. Empirical refinement of the SOC water-holding coefficient at Pakistan-specific soil textures, alongside in-situ flux-tower measurement of pre-monsoon ET response to amendment trials, would substantially reduce the uncertainty on Lever 1B's contribution.

Acknowledgments

ERA5 data were obtained from the Copernicus Climate Data Store. The author declares no conflicts of interest.

Open Research

Reanalysis and observational data. ERA5 single-level fields [Hersbach et al., 2020] were obtained via the Copernicus Climate Data Store [Copernicus Climate Change Service, 2023]. MERRA-2 hourly surface fields (M2T1NXSLV) [Gelaro et al., 2017] were retrieved from NASA GES DISC via OPeNDAP. IGRA v2 radiosonde records [Durre et al., 2018] were downloaded from NOAA NCEI's public archive (`https://www.ncei.noaa.gov/products/weather-balloon/integrated-global-radiosonde-archive`). GLDAS-2.1 NOAH monthly fields [Rodell et al., 2004] were retrieved from NASA GES DISC. NASA GPM IMERG V07 half-hourly precipitation [Huffman et al., 2023] was retrieved from NASA GES DISC via OPeNDAP. GRACE/GRACE-FO JPL MASCON RL06 v04CRI was obtained from NASA JPL.

Land-cover products. ESA WorldCover 2021 (10 m, v200) [Zanaga et al., 2022] was obtained from the ESA WorldCover Zenodo distribution (`https://doi.org/10.5281/zenodo.7254221`). Hansen Global Forest Change v1.11 [Hansen et al., 2013] was obtained from the GLAD (`https://glad.umd.edu/dataset/global-2010-tree-cover-30-m`). ESA CCI Land Cover [Defourny et al., 2018] was obtained via the ESA Climate Change Initiative portal.

Analysis code and derived data. The full analysis pipeline (Python scripts, derived intermediate products, configuration files, and figure-generation code) is archived on GitHub (`https://github.com/R3GENESI5/pakistan-orographic-water-potential`) and mirrored on Zenodo (`https://doi.org/10.5281/zenodo.20176557`).

References

G. Ali, G. Rasul, Q. Mahmood, et al. Spatial–temporal characterization of rainfall in Pakistan during the past half-century (1961–2020). *Scientific Reports*, 2021. doi: 10.1038/s41598-021-86412-x.

D. R. Archer and H. J. Fowler. Spatial and temporal variations in precipitation in the Upper Indus Basin, global teleconnections and hydrological implications. *Hydrology and Earth System Sciences*, 8:47–61, 2004. doi: 10.5194/hess-8-47-2004.

D. Bolton. The computation of equivalent potential temperature. *Monthly Weather Review*, 108(7):1046–1053, 1980. doi: 10.1175/1520-0493(1980)108<1046:TCOEPT>2.0.CO;2.

G. B. Bonan. Forests and climate change: Forcings, feedbacks, and the climate benefits of forests. *Science*, 320(5882):1444–1449, 2008. doi: 10.1126/science.1155121.

B. Bookhagen and D. W. Burbank. Toward a complete Himalayan hydrological budget: Spatiotemporal distribution of snowmelt and rainfall and their impact on river discharge. *Journal of Geophysical Research: Earth Surface*, 115:F03019, 2010. doi: 10.1029/2009JF001426.

Copernicus Climate Change Service. ERA5: Fifth generation of ECMWF atmospheric reanalyses of the global climate, Copernicus Climate Change Service Climate Data Store (CDS). https://cds.climate.copernicus.eu, 2023.

P. Defourny, C. Lamarche, S. Bontemps, T. De Maet, E. Van Bogaert, I. Moreau, C. Brockmann, M. Boettcher, G. Kirches, J. Wevers, M. Santoro, F. Achard, J. Eberle, and S. Plummer. Land Cover CCI: Algorithm Theoretical Basis Document, version 2.3. Document reference: Cci-lc-ph2-atbdv2.3, European Space Agency Climate Change Initiative, 2018. URL https://climate.esa.int/media/documents/Land_Cover_CCI_ATBDv2_2.3.pdf.

A. P. Dimri, D. Niyogi, A. P. Barros, J. Ridley, U. C. Mohanty, T. Yasunari, and D. R. Sikka. Western disturbances: A review. *Reviews of Geophysics*, 53(2):225–246, 2015. doi: 10.1002/2014RG000460.

I. Durre, X. Yin, R. S. Vose, S. Applequist, and J. Arnfield. Enhancing the Data Coverage in the Integrated Global Radiosonde Archive. *Journal of Atmospheric and Oceanic Technology*, 35(9):1753–1770, 2018. doi: 10.1175/JTECH-D-17-0223.1.

D. Ellison, C. E. Morris, B. Locatelli, et al. Trees, forests and water: Cool insights for a hot world. *Global Environmental Change*, 43:51–61, 2017. doi: 10.1016/j.gloenvcha.2017.01.002.

K. L. Findell and E. A. B. Eltahir. Atmospheric controls on soil moisture–boundary layer interactions. Part I: Framework development. *Journal of Hydrometeorology*, 4:552–569, 2003. doi: 10.1175/1525-7541(2003)004<0552:ACOSML>2.0.CO;2.

Food and Agriculture Organization of the United Nations. Global forest resources assessment 2020: Country report – pakistan. Technical report, FAO, Rome, 2020a.

Food and Agriculture Organization of the United Nations. Pakistan: National aquaculture sector overview and agricultural water use. Technical report, FAO, Rome, 2020b.

R. Gelaro, W. McCarty, M. J. Suárez, R. Todling, A. Molod, L. Takacs, C. A. Randles, A. Darmenov, M. G. Bosilovich, R. Reichle, K. Wargan, L. Coy, R. Cullather, C. Draper, S. Akella, V. Buchard, A. Conaty, A. M. da Silva, W. Gu, G.-K. Kim, R. Koster, R. Lucchesi, D. Merkova, J. E. Nielsen, G. Partyka, S. Pawson, W. Putman, M. Rienecker, S. D. Schubert, M. Sienkiewicz, and B. Zhao. The Modern-Era Retrospective Analysis for Research and Applications, Version 2 (MERRA-2). *Journal of Climate*, 30(14):5419–5454, 2017. doi: 10.1175/JCLI-D-16-0758.1.

M. C. Hansen, P. V. Potapov, R. Moore, M. Hancher, S. A. Turubanova, A. Tyukavina, D. Thau, S. V. Stehman, S. J. Goetz, T. R. Loveland, A. Kommareddy, A. Egorov, L. Chini, C. O. Justice, and J. R. G. Townshend. High-resolution global maps of 21st-century forest cover change. *Science*, 342(6160):850–853, 2013. doi: 10.1126/science.1244693.

H. Hersbach, B. Bell, P. Berrisford, et al. The ERA5 global reanalysis. *Quarterly Journal of the Royal Meteorological Society*, 146(730):1999–2049, 2020. doi: 10.1002/qj.3803.

R. A. Houze. Orographic effects on precipitating clouds. *Reviews of Geophysics*, 50(1): RG1001, 2012. doi: 10.1029/2011RG000365.

R. A. Houze, K. L. Rasmussen, S. Medina, S. R. Brodzik, and U. Romatschke. Anomalous atmospheric events leading to the summer 2010 floods in pakistan. *Bulletin of the American Meteorological Society*, 92(3):291–298, 2011. doi: 10.1175/2010BAMS3173.1.

B. D. Hudson. Soil organic matter and available water capacity. *Journal of Soil and Water Conservation*, 49(2):189–194, 1994.

G. J. Huffman, E. F. Stocker, D. T. Bolvin, E. J. Nelkin, and J. Tan. GPM IMERG Final Precipitation L3 Half Hourly 0.1 degree x 0.1 degree V07, 2023.

M. Hussain, M. Yusuf, Q. Mahmood, et al. Observed trends and variability of seasonal and annual precipitation in Pakistan during 1960–2016. *International Journal of Climatology*, 2022. doi: 10.1002/joc.7709.

W. W. Immerzeel, A. F. Lutz, M. Andrade, et al. Importance and vulnerability of the world's water towers. *Nature*, 577:364–369, 2020. doi: 10.1038/s41586-019-1822-y.

B. Ingleby. An assessment of different radiosonde types 2015/2016. ECMWF Technical Memorandum 807, European Centre for Medium-Range Weather Forecasts, Reading, United Kingdom, 2017. URL https://www.ecmwf.int/sites/default/files/elibrary/2017/17551-assessment-different-radiosonde-types-20152016.pdf.

D. J. Kirshbaum, B. Adler, N. Kalthoff, C. Barthlott, and S. Serafin. Moist orographic convection: Physical mechanisms and links to surface-exchange processes. *Atmosphere*, 9 (3):80, 2018. doi: 10.3390/atmos9030080.

R. Krishnan, A. B. Shrestha, G. Ren, et al. Unravelling climate change in the Hindu Kush Himalaya: Rapid warming in the mountains and increasing extremes. In P. Wester, A. Mishra, A. Mukherji, and A. B. Shrestha, editors, *The Hindu Kush Himalaya Assessment*, pages 57–97. Springer, Cham, 2019. doi: 10.1007/978-3-319-92288-1_3.

J. Lehmann and S. Joseph, editors. *Biochar for Environmental Management: Science, Technology and Implementation*. Routledge, London, 2nd edition, 2015. doi: 10.4324/9780203762264.

A. F. Lutz, W. W. Immerzeel, A. B. Shrestha, and M. F. P. Bierkens. Consistent increase in High Asia's runoff due to increasing glacier melt and precipitation. *Nature Climate Change*, 4:587–592, 2014. doi: 10.1038/nclimate2237.

A. M. Makarieva and V. G. Gorshkov. Biotic pump of atmospheric moisture as driver of the hydrological cycle on land. *Hydrology and Earth System Sciences*, 11:1013–1033, 2007. doi: 10.5194/hess-11-1013-2007.

J. S. Nanditha, A. P. Kushwaha, R. Singh, et al. The Pakistan flood of August 2022: Causes and implications. *Earth's Future*, 11, 2023. doi: 10.1029/2022EF003230.

E. Palazzi, J. von Hardenberg, and A. Provenzale. Precipitation in the Hindu-Kush Karakoram Himalaya: Observations and future scenarios. *Journal of Geophysical Research: Atmospheres*, 118:85–100, 2013. doi: 10.1029/2012JD018697.

M. Rodell, P. R. Houser, U. Jambor, J. Gottschalck, K. Mitchell, C.-J. Meng, K. Arsenault, B. Cosgrove, J. Radakovich, M. Bosilovich, J. K. Entin, J. P. Walker, D. Lohmann, and D. Toll. The Global Land Data Assimilation System. *Bulletin of the American Meteorological Society*, 85(3):381–394, 2004. doi: 10.1175/BAMS-85-3-381.

G. H. Roe. Orographic precipitation. *Annual Review of Earth and Planetary Sciences*, 33: 645–671, 2005. doi: 10.1146/annurev.earth.33.092203.122541.

D. M. Romps. Exact expression for the lifting condensation level. *Journal of the Atmospheric Sciences*, 74(12):3891–3900, 2017. doi: 10.1175/JAS-D-17-0102.1.

R. B. Smith. The influence of mountains on the atmosphere. *Advances in Geophysics*, 21: 87–230, 1979. doi: 10.1016/S0065-2687(08)60262-9.

D. V. Spracklen, J. C. A. Baker, L. Garcia-Carreras, and J. H. Marsham. The effects of tropical vegetation on rainfall. *Annual Review of Environment and Resources*, 43:193–218, 2018. doi: 10.1146/annurev-environ-102017-030136.

M. Tahir, A. Farooqi, and G. Rasul. Impact assessment of orography on the extreme precipitation event of July 2010 over Pakistan: A numerical study. *Advances in Meteorology*, 2015. doi: 10.1155/2015/510417.

R. P. Tucker. The british colonial system and the forests of the western Himalayas, 1815–1914. *Global Ecology and Biogeography Letters*, 10:3–19, 1983.

O. A. Tuinenburg, R. W. A. Hutjes, and P. Kabat. The fate of evaporated water from the Ganges basin. *Journal of Geophysical Research: Atmospheres*, 117(D1), 2012. doi: 10.1029/2011JD016221.

United Nations. System of environmental-economic accounting – ecosystem accounting (SEEA EA). Technical report, United Nations Statistical Division, New York, 2021.

Water and Power Development Authority (Pakistan). Indus river system water apportionment and groundwater status report. Technical report, WAPDA, Lahore, Pakistan, 2021.

P. J. Webster, V. E. Toma, and H.-M. Kim. Were the 2010 pakistan floods predictable? *Geophysical Research Letters*, 38(4):L04806, 2011. doi: 10.1029/2010GL046346.

J. Westoby. *The Purpose of Forests: Follies of Development*. Basil Blackwell, Oxford, 1987.

World Bank. Pakistan floods 2022: Post-disaster needs assessment. Technical report, World Bank Group, Washington, DC, 2022.

World Meteorological Organization. The Global Observing System for Climate: Implementation Needs (GCOS-200). Technical report, World Meteorological Organization, Geneva, Switzerland, 2016. URL https://gcos.wmo.int/site/global-climate-observing-system-gcos/publications.

D. Zanaga, R. Van De Kerchove, D. Daems, W. De Keersmaecker, C. Brockmann, G. Kirches, J. Wevers, O. Cartus, M. Santoro, S. Fritz, M. Lesiv, M. Herold, N.-E. Tsendbazar, P. Xu, F. Ramoino, and O. Arino. Esa worldcover 10 m 2021 v200, 2022.